Effect of operating conditions and feedstock composition on the properties of manganese oxide or quartz charcoal pellets for the use in ferroalloy industries

Gerrit Ralf Surup, Henrik Kofoed Nielsen, Marius Großarth, Rüdiger Deike, Jan Van den Bulcke, Pierre Kibleur, Michael Müller, Mirko Ziegner, Elena Yazhenskikh, Sergey Beloshapkin, James J. Leahy, Anna Trubetskaya

Effect of operating conditions and feedstock composition on the properties of manganese oxide or quartz charcoal pellets for the use in ferroalloy industries

Gerrit Ralf Surup[a], Henrik Kofoed Nielsen[b], Marius Großarth[c], Rüdiger Deike[c], Jan Van den Bulcke[d], Pierre Kibleur[e], Michael Müller[f], Mirko Ziegner[f], Elena Yazhenskikh[f], Sergey Beloshapkin[g], James J. Leahy[g], Anna Trubetskaya[g,*]

[a]*Department of Materials Science and Engineering, Norwegian University of Science and Technology, 7491, Trondheim, Norway*
[b]*Department of Engineering Sciences, University of Agder, 4879 Grimstad, Norway*
[c]*Chair of Metallurgy for Iron and Steel Production, University of Duisburg-Essen, 47119 Duisburg, Germany*
[d]*Laboratory of Wood Technology - Woodlab, Gent University, 9000, Gent, Belgium*
[e]*Department of Physics and Astronomy, Gent University, 9000, Gent, Ireland*
[f]*Institute of Energy and Climate Research, Jülich Research Centre, 52428 Jülich, Germany*
[g]*Bernal Center, University of Limerick, Castletroy, Ireland*

Abstract

This study investigates the effect of heat treatment temperature on the properties of charcoal composite pellets used for the reduction of ferroalloys. The heavy fraction of biooil was used as a binder for the charcoal ore pellet preparation. The effect of heat treatment temperature on the pellet shrinkage was related to the degree of reduction which varied with feedstock and ore composition. The results showed that the size and shape of the charcoal pellets were not affected by the biooil devolatilization. Manganese charcoal pellets showed higher electrical resistance during pyrolysis, whereas the structure,

*Corresponding author. anna.trubetskaya@ul.ie

composition and electrical resistance of silica composite pellets remained unaffected by heat treatment temperatures < 1650°C. However, the secondary heat treatment decreased the CO_2 gasification reactivity and electrical resistivity of charcoal composite pellets. In addition, the findings of this work demonstrate the potential for using biooil as a binder for the charcoal composite pellets used in ferroalloy industries. The composite pellets are suitable to pre-reduce the manganese ore in the low temperature zones of an industrial furnace, and the charcoal pellets can be used as an alternative bed material. However, the high CO_2 reactivity may create challenges during the direct replacement of metallurgical coke with the bio-reductants.
Keywords: charcoal, ferroalloys, biooil, ash, pyrolysis

1. Introduction

Metallurgy is one of the most energy intensive industries, and is responsible for about 10 % of the global anthropogenic CO_2 emissions [1]. The use of biomass and its derivatives as CO_2 neutral reducing agents in metallurgical processes can provide a possible solution to decrease emissions [2]. One of the challenges in using charcoal in metallurgical processes is related to its fragility with the generation of large amounts of fine particles during transportation and storage [3]. The mechanical strength of charcoal can be improved through pelletization or briquetting [4, 5]. In the ferroalloy industries, manganese ore pellets must be sintered at higher temperatures to provide mechanical stability similar to that of iron ore pellets. The addition of sawdust and dolomite are known to increase the required sintering temperature of the ore pellets [6, 7]. Current metallurgical production is based

on the use of fossil-based fuels because the use of charcoal-ore pellets in the reduction process can increase the overall power consumption by 72-152 kWh per tonne of FeMn and will increase the cost of a reduction process [8, 9].

The properties of charcoal pellets can be affected by the feedstock, particle size and pelletization process. A uniform pellet size improves the gas permeability of the bed material and the heat exchange between the hot gases and the charge, leading to furnace stable operation [10]. The high porosity of charcoal pellets affects the mechanical strength and degree of pre-reduction, whereas the shape factor and size of a carbonaceous pellet has a strong influence on the segregation and gas permeability during ore reduction. The early stages of the reduction process depend on the mass transfer between the solid carbon and metal oxide [11]. Thus, a small carbon charge results in high pre-reduction of ore metals and decreased heat treatment temperature, which might also affect the temperature in a coke bed [12]. In addition, fine charcoal particles can lead to a poor gas permeability in the burden. Similar problems can occur when the melting temperature is below the reduction temperature and no contact exists between the molten metal-oxide and the coke bed [13]. Moreover, the melting temperature of minerals can affect furnace temperature zones, with an increased content of acid oxides decreasing the melting temperature of ore metals [8, 14]. The carbon must be optimized the direct reduction of iron ore composite pellets is required to be below the stoichiometric amount of carbon required for the reduction [15]. Charcoal pellets with high volatile content could lead to elevated release of volatile matter, resulting in increased porosity and the formation of cracks during material reduction [15, 16]. In addition, the low mechanical stability,

high reactivity and shrinkage of charcoal particles might create challenges for the stable operation of the furnace [17, 18]. Starch activated with a small amount of moisture and used as a binder in charcoal composite pellet improved the pellet mechanical strength [19]. Moreover, the use of pyrolysis oil as a binder in charcoal composite pellets was shown to provide the water required for the pelletization process and also to form oxygen-containing functional groups which increase the mechanical strength of pellets due to the ability to form hydrogen bonds during pyrolysis [5, 20]. The additional heat treatment of charcoal composite pellets using biooil as a binder was shown to decrease the charcoal pellet porosity due to the repolymerization of biooils in the macropores of charcoal pellets [4]. Moreover, recent studies have shown that the use of pyrolysis oil as a binder, instead of lignin and starch, can decrease process operating costs of charcoal pellet production and also improve the densification of charcoal during storage and transportation [21, 22]. The reduction of charcoal composite pellets results in a significant change in the properties and shape of pellets in the ferroalloy industries [23, 24]. In previous studies, dilatation of iron composite pellets was observed in the temperature range from 900 to 1000°C due to whisker growth, whereas shrinkage occurred in the temperature range from 1100 to 1200°C due to sintering of iron filaments [25, 26]. In addition, the swelling of iron composite pellets at temperatures below 1100°C is correlated with the transition from iron oxide to the elemental metal [7]. The volume of composite pellets can also change due to the variation of the temperature gradient which is affected by exothermic and endothermic reactions in the pellet during reduction, leading to the unstable operation of the furnace [27]. Swelling of composite pellets

increases the apparent porosity and decreases the mechanical stability [28]. Concurrently, the mechanical stability can also decrease, resulting in an increased formation of dust and fines [25]. The fine particles decrease the gas permeability of the bed and may cause pressure surges which cause the unreacted particles to blow out of the bed [29]. The reduction of hematite ore fines by different fossil-based carbonaceous materials in composite pellets in a one-layer bed under nonisothermal asymmetric heating showed that the reduction is faster at the pellet top compared to the pellet bottom [30]. In addition, the pellets with the greater initial volatile content but with the same amount of fixed carbon gave a significantly greater degree of reduction without the involvement of the fixed carbon gasification reaction [31, 32]. The replacement of anthracite fines with charcoal prepared from eucalyptus showed that low temperature pre-treatment of wood decreases the volatile content leading to a decrease macropores and an improvement of pellet mechanical strength and durability [33]. Moreover, the mechanical strength and electrical resistance of fossil-based pellets with the included iron ore were increased with the addition of carbonized leather charcoal [34]. The principal strengthening mechanism of heated charcoal composite pellets from biomass was related to the formation of interconnecting slag and metallic phases during reduction [35, 36]. Processing parameters, such as increasing heat treatment temperature and the addition of fluxes increased slag formation [37]. In addition, the distance between iron oxide particles decreased with the increasing iron-to-carbon ratio in charcoal composite pellets and decreased charcoal particle size leading to an increase in pellet mechanical strength during reduction [38]. The change in pellet volume during reduction

of charcoal composite pellets with the iron ore inclusions was related to the heat treatment temperature and size of pellets [39, 40]. However, the effects of the charcoal properties and composition on the resulting composite pellet characteristics that impact metallurgical applications add uncertainty to the use of bio-reductants as an approach to increasing yields of manganese or silicon during reduction of metal oxides.

In summary, renewable charcoal pellets have potential as an environmentally benign replacement for the fossil-based composite pellets used in ferroalloy production. In particular, this work was intended to investigate the interaction of charcoal with the metal ore under high temperatures. The aim of this work is to optimize the operating conditions for the cost-effective bioreductant pellet production from wood to provide properties which are similar to metallurgical coke pellets. In this study, the impacts of charcoal composition on the density, thermal conductivity and elemental metal yields during reduction in a high temperature furnace were investigated. The specific objectives of this study were to: (1) understand the influence of reduction process on the properties of charcoal composite pellets, (2) investigate the interaction of charcoal composite pellets with the included metal ore particles at high temperatures and (3) determine the extent to which charcoal composite pellet reduction changes its properties to levels that are suitable for application in ferroalloy industries.

2. Materials and methods

2.1. Raw biomass characterization

Norway spruce (*Picea abies*) and sessile oak (*Quercus petraea*) were chosen for the charcoal composite pellet study. The age of the Norway spruce was 39 years, whereas the oak was 46 years old. Feedstock selection was based on the differences in ash composition and compositional analysis (cellulose, hemicellulose, lignin, extractives) of softwood and hardwood. Norway spruce is low in ash, with lower potassium and calcium contents than oak, whereas oak is low in lignin content. Both spruce and oak samples were chipped by a disc chipper to 5-20 mm and dried at 60°C before storage. Prior to the wood characterization, the biomass samples were divided into six equal fractions using a riffler. A vibrating EFL2000 sieve shaker (ENDECOTTS, United Kingdom) comprising ten sieves ranging from 2 to 20 mm in aperture size and a base pan (< 2 mm) was used (EN ISO 17827-2:2016) to determine the particle size distribution.

2.2. Charcoal characterization

Charcoal samples from Norway spruce and sessile oak were generated from woodchips in a slow pyrolysis reactor at 500, 700, 900, 1100 and 1300°C. The charcoal samples were crushed to a fine powder in a mortar with a ceramic pestle and used for heating microscopy and thermogravimetric analysis tests. A charcoal sample from Norway spruce produced at 900°C was chosen for the reduction in a high temperature furnace. Based on previous work [41, 42], operation at 900°C was selected to produce the charcoal cost-efficiently with properties comparable to that of metallurgical coke. Biooil

from the slow pyrolysis experiments was selected as the binding agent. Prior to pelletization, the water fraction of the biooil was removed by vacuum distillation (300 mbar and 80°C) and the residual (tar), was used as a binder. A compact hot pellet press (MTI Corporation, USA), consisting of a metal cylinder with a press channel, a backstop and a split furnace was used for preparing the pellets. Charcoal pellets were made from charcoal particles, tar binder and water in a 60:30:10 wt.% ratio. Composite pellets were prepared from high purity manganese ore (Eramet AS, Norway), charcoal, tar and water in a 46:14:30:10 wt.% ratio, whereas microsilica particles (Elkem AS, Norway) were mixed with the charcoal, tar and water in a 30:30:30:10 wt.% ratio. The mixing ratios were selected according to the ratios of ore and coke used in the industrial process. Pellets with a diameter and height of 3 mm were pressed using a manual pellet press (Hesse instruments, Germany). About 3 g of the mixture was pressed at 130 MPa into pellets with a diameter of 12 mm and a height of about 20 mm. Once the pellet was pressed, the backstop was removed and the pellet was extruded from the steel die. The pellets were dried at 30°C overnight in a drying chamber and stored in sealed plastic containers.

2.3. High-temperature furnace

The charcoal was treated in a vacuum induction furnace (max. 60 kW, max. 10 kHz) with a chamber volume of 0.5 m^3. The heating vessel consisted of a three-part crucible with an outer alumina crucible (outer diameter: 130 mm, inner diameter: 110 mm, height: 300 mm), a middle carbon crucible (outer diameter: 90 mm, inner diameter: 50 mm, height: 145 mm) and an inner glass carbon crucible (outer diameter: 50 mm, inner diameter: 38 mm,

height: 125 mm), as described previously [41]. The three-part crucible was positioned in an induction coil. The gap between the alumina crucible and the carbon crucible was filled with a carbon felt. A carbon felt disc (diameter: 110 mm, height: 30 mm) was placed between the bottom of the alumina and carbon crucibles was used for the high-temperature protection. The pellets were placed in the glassy carbon crucible. The pellets were placed in the glassy carbon crucible. The pellet temperature was measured using type S thermocouples about 5 mm above each pellet. Prior to the experiment, the chamber was evacuated and filled with argon. The chamber was continuously purged with argon at a defined flow rate of 20 l min^{-1}. The formation of carbon monoxide was monitored using by a gas emission analyser, VARIO Luxx (MRU, Germany). The sample was heated to 900°C at a heating rate of 100°C min^{-1} and further heated at 10°C min^{-1} to 1650°C and maintained kept at that temperature for 2 h. After the heating program was finished, the sample was cooled at a rate of 30°C min^{-1} to room temperature and stored in sealed plastic containers.

2.4. Solid product analysis

2.4.1. Thermogravimetric analysis

The reactivity the milled charcoal and charcoal pellets were analyzed by exposing samples to a reactive gas consisting of 100 % volume fraction of CO_2 (100 cm^3 min^{-1}) in a thermogravimetric analyser TGA/DSC System (Mettler Toledo, USA). In each experiment, 5 mg of sample was loaded into an Al_2O_3 crucible. The charcoal samples were firstly heated to 110°C and kept for 30 min isothermally for drying. The dried samples were subsequently heated to 1100°C at a constant heating rate of 10°C min^{-1} and

maintained at the final temperature for 30 min. The reaction threshold is defined as the temperature that corresponds to the appearance of a sample mass decrease [43]. Non-isothermal thermogravimetric measurements were carried out in 100 vol.% N_2 to determine the thermal decomposition of charcoal samples and to distinguish between pyrolysis and gasification reactions at medium and elevated temperatures.

2.4.2. Heating microscopy

The silhouettes of charcoal pellets were investigated in inert atmosphere using an EM-201-17 (Hesse Instrument, Germany) heating microscope, as shown in Figure 1.

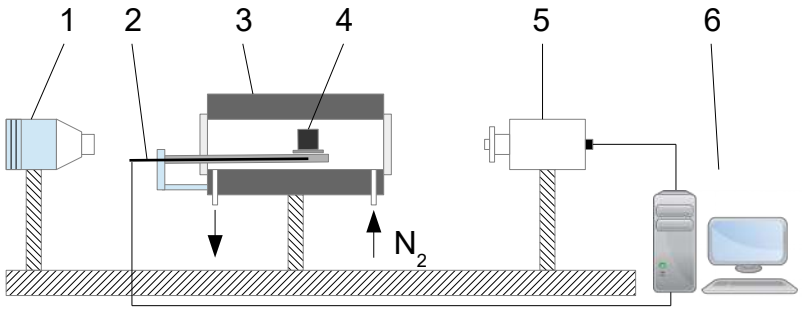

Figure 1: Heating microscope includes the following parts: 1. Light source, 2. Thermocouple type S, 3. Heating chamber, 4. Charcoal pellet sample, 5. Camera, 6. Computer.

Charcoal pellets with a diameter and height of 3 mm were used for the experiments. The charcoal pellets with an edge length of 3 or 4 mm were placed in the center of the sample plate above the tip of the thermocouple. The heating chamber was continuously purged with nitrogen at a constant

rate of 500 ml min^{-1}, which was controlled by a flowmeter HFC-202 (Teledyne, USA). The samples were heated to 500°C at a constant heating rate of 30°C min^{-1} and further heated at a heating rate of 10°C min^{-1} to the final temperature of 1300°C, and maintained for 30 min.

2.4.3. Electrical resistivity

Electrical conductivity measurements were performed using a 34470A 7 1/2 Digit Multimeter (Keysight Technologies, USA). The connection between the four probes of the source meter and microelectrodes was established using a socket. Two adjacent electrodes were connected to the voltmeter (Fluke, USA), while the other two electrodes were connected to the current source (ISO-Tech IPS 3303) (constant current) of the source meter, as reported by Sun et al. [44]. A charcoal pellet was connected by four different electrodes to the source meter based on the van der Pauw electrode geometry [45]. The electrical conductivity was determined according to equation 1:

$$\sigma = \frac{L}{R \cdot A} \tag{1}$$

In equation 1, σ is the electrical conductivity, A is the cross-sectional area, L is the length of the resistor, and R is the resistance between Ti-Au electrodes.

2.4.4. Microscopy

The surface properties of the charcoal composite pellets were investigated using a digital microscope VHX-500F (Keyence, Germany), and the cross-sections of samples were analyzed using an optical microscope DM4000 M LED (Leica, Germany). Prior to the analysis, the composite pellets were embedded in the conductive polymer Technovit® 5000 (Kulzer Technik, Germany). SEM/EDS analysis of the char was conducted on a high-resolution

field emission microscope SU-70 (Hitachi, Japan) under high vacuum in order to understand the structural properties and composition of the ferroalloys and charcoal pellets. The elemental mapping was performed on four different areas of interest for the manganese oxides and quartz charcoal pellets.

2.4.5. Thermodynamic calculations

Thermodynamic calculations were performed using the computational package FactSage [46]. The new oxide database GTOX, developed by Research Center Juelich and GTT-Technologies as reported by Yazhenskikh et al. [47] was used in combination with the commercial database SGPS for gaseous and some solid stoichiometric substances. The equilibrium calculations were conducted under defined conditions (chemical composition of a system, temperature, pressure) [48]. All available phase relations and transformations were taken into account during the calculation of the minimized Gibbs energy of a system in order to find the equilibrium state. The results were obtained for equilibrium conditions only, the possible kinetic effects are not considered.

2.5. X-ray diffraction

The crystalline constituents of charcoal and charcoal composite pellets were characterized using an Empyrean X-ray diffractometer (Malvern Panalytical, The Netherlands) in parafocusing Bragg-Brentano geometry (setup: Cu LFF tube operated at 40 kV and 40 mA, BBHD-mirror with 0.4° divergence, 0.04 rad soller slits, PIXcel3D detector in 1D mode). The samples were placed on a background-free Si single crystal sample holder. The phase analyses were done in the HighScore software package Version 4.8 (Malvern

Panalytical, The Netherlands) and the ICDD PDF-2 database 2004 (International Centre for Diffraction Data, USA).

2.5.1. X-ray microtomography

The pellets were scanned using the HECTOR X-ray CT system at the Ghent University Centre for X-ray Tomography (UGCT, www.ugct.ugent.be) [49, 50]. The HECTOR system was developed and built by the Radiation Physics group of the UGCT in collaboration with TESCAN XRE, (www.XRE.be, part of the TESCAN ORSAY HOLDING a.s.), formerly known as XRE, a UGCT spin-off company.

Charcoal pellets. A Region of Interest (ROI) of both an untreated and a treated charcoal pellet was scanned without physical subsampling to avoid any cutting artifacts. The X-ray tube voltage and tube power were 70 kV and 10 W, respectively. 2401 projections, with an exposure time of 1 s per projection, were collected over a sample rotation of 360°, for a total scan duration of 1 h. The volumes were reconstructed using the Octopus Reconstruction software [51], licensed by XRE, and the spatial resolution in terms of approx- imate voxel pitch was 3.5 μm. The reconstructed pellet structure corresponds to a cylinder with a diameter of 6.7 mm and a height of 5.9 mm. In order to calculate the porosity within the pellet volume, segmentation was carried out by interactive thresholding with a visual feedback using Avizo software (Thermo Fisher Scientific, USA). The latter software was also used for rendering the 3D visualizations.

Composite pellets. Composite pellets containing either manganese (Z=25) or silicon (Z=14) were scanned differently due to the poor X-ray penetration

of the samples. Tube voltage and tube power were 130 kV and 10 W respectively. 2401 projections, with an exposure time of 2 s per projection, were collected over a sample rotation of 360°, for a total scan duration of 1.5 h. The volumes were also reconstructed with Octopus Reconstruction software, yielding a voxel size of 4 μm. The analysis of the heat-treated manganese ore pellet in a reconstructed cylinder form with a diameter of 8 mm and height of 6.5 mm was not conducted due to the fragile nature of the pellet. However, a reconstructed cylinder of diameter 6.5 mm and height 6.5 mm that corresponded to the inner dimensions of a plastic tube in which the pellet was mounted for scanning was used in the present work. Due to the high contrast between the different solid phases in composite pellets, it was no longer possible to calculate the porosity. Instead, interactive thresholding was applied to visualize a segment with the high density voxels in the original charcoal pellet scans. The same threshold was used to segment the high density voxels in the heat treated pellet scans and thus, an estimate of change in the relative proportion of heavy elements (namely Mn and Si) after heat treatment was calculated.

3. Results and discussion

3.1. Biomass characterization

The ultimate and proximate analysis of oak and spruce was carried out at Eurofins Lidköping and shown in Table 1.

Table 1: Proximate, ultimate and ash analyses of feedstocks.

Fuel	Norway spruce	Oak
Proximate analysis		
Moisture, (wt. % as received)	8.6	7.6
Ash at 550 °C, (wt. % dry basis)	0.8	1.6
Volatiles, (wt. % dry basis)	80.6	82.6
Fixed carbon content (wt. % dry basis)	18.6	15.8
HHV, (MJ kg^{-1})	20.3	19.3
LHV, (MJ kg^{-1})	18.5	17.5
Ultimate analysis, (wt. %, dry basis)		
C	53.2	50.6
H	6.1	6.1
N	0.1	0.2
S	0.06	0.02
Cl	0.04	0.02
Ash compositional analysis, (mg kg^{-1} on dry basis)		
Al	40	20
Ca	2300	3600
Fe	200	50
K	800	1500
Mg	250	300
Na	<50	<50
P	200	250
Si	550	550
Ti	50	50

The compositional analysis of biomass (cellulose, hemicellulose, acid-soluble lignin, acid-insoluble lignin, and extractives) was conducted by Celignis Analytical according to NREL technical reports [52–54] and Thammasouk et al. [55], and is shown in Table 2.

Table 2: Composition of Norway spruce and oak, calculated in percentage based on dry basis (wt. %).

Biomass	**Cellulose**	**Hemicellulose**	**Lignin**		**Extractives**
			acid insoluble	**acid soluble**	
Norway spruce	37.8	25	27.9	0.7	7.8
Oak	36.7	18.7	19.4	2.5	11

3.2. Product yields

The original spruce and oak charcoal pellets and charcoal composite pellets from pyrolysis at temperatures ranging from 500 to 1300°C were reacted in a heating microscope in order to investigate the behaviour of the pellets at high temperatures. The mass losses at 1200°C from tests using heating microscopy were recorded. In addition, the mass losses of manganese and quartz charcoal pellets were determined in the high-temperature furnace at 1550 and 1650°C, as shown in Figure 2. The results show that the mass loss from secondary pyrolysis of both spruce and oak charcoal pellets decreased with increasing primary pyrolysis temperature, from about 55 % for charcoal produced at 500°C to 11 % for charcoal generated at 1300°C. Prior to reduction, the charcoal composite pellet contained 46 wt.% manganese ore and 54 wt.% charcoal matrix. This suggests that almost all of the organic fraction of the charcoal composite pellet reacted at 500°C. The increased yield of quartz charcoal composite pellets from about 30 % for charcoal produced at 500°C to 37 % for charcoal generated at 1300°C suggests the formation of slag. The pellet prepared from quartz, charcoal, tar and water in a 30:30:30:10 wt.% ratio could include interactions of quartz particles with the alkali metals in

a charcoal matrix, leading to the formation of an interconnecting slag with the increased heat treatment temperature [35, 36].

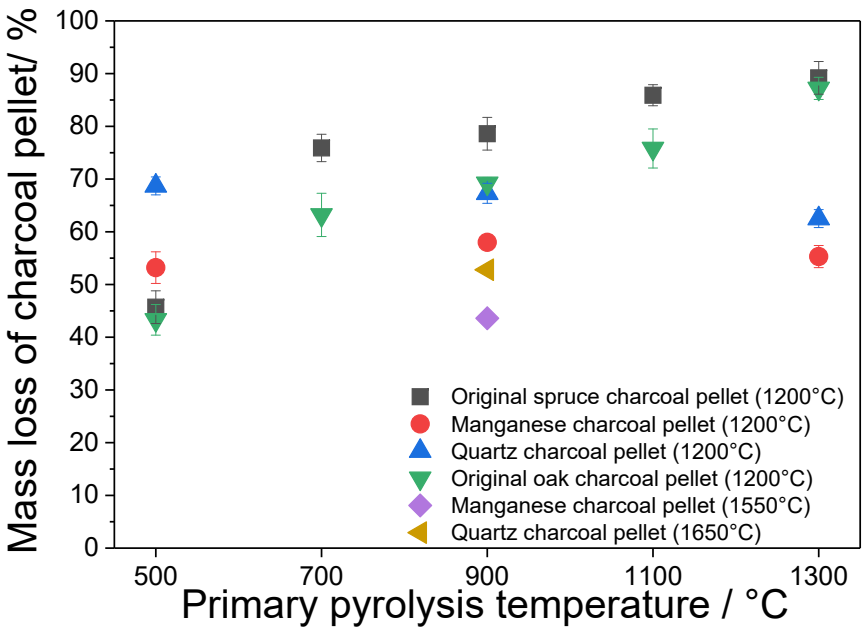

Figure 2: Charcoal pellet yields (%) from secondary pyrolysis in a heating microscope and high-temperature furnace.

In general, the mass loss of the original charcoal pellets was greater than the mass loss of secondary heat treated charcoal particles which decreased from about 22 % for the charcoal produced at 500°C to 6 % for charcoal generated at 1300°C [41]. The greater mass loss of charcoal pellets compared to that of the original charcoal particles was attributed to the high binder and water contents in the pellets. In addition, the pellet from charcoal produced at 1300°C showed the greatest solid yield, indicating enhanced coke formation from reacting biooil in a charcoal matrix. This was related to the increase in

porosity of the charcoal due to the progressive removal of volatiles from the pores, and the physical and chemical condensation of the remaining skeletal charcoal structure with increasing heat treatment temperature, confirming the previous results [56, 57]. Consequently, the charcoal particles with greater porosity had a stronger tendency to trap reacting biooil in voids than the charcoal produced at heat treatment temperatures below 1300°C, confirming previous results of Veksha et al. [58]. The solid pellet yields of composite pellets remained similar for the charcoal produced at 500, 900 and 1300°C, indicating competition between devolatilization and reduction reactions. In addition, the solid yields for the composite pellets were lower than those of original charcoal pellets. This is probably due to the competing reduction and devolatilization reactions in pyrolysis of charcoal composite pellets [59].

3.3. Gas evolution

The gas evolution from the composite pellets is shown in Figure 3. At 900°C, the heating rate of 100°C min^{-1} was changed to 10°C min^{-1}, leading to the decrease in a gas volume. The formation of CO was shifted to lower temperatures due to the endothermic reactions which decrease the decomposition temperature of composite pellets. Gas evolution at temperatures below 1000°C was attributed to devolatilization and decomposition of biooil and reduction of higher oxides, such as the reduction of MnO_2 to Mn_3O_4. The main CO formation during the heat treatment of manganese ore composite pellets was observed at temperatures above 1020°C with a maximum formation at 1480°C, confirming previous results [8, 60].

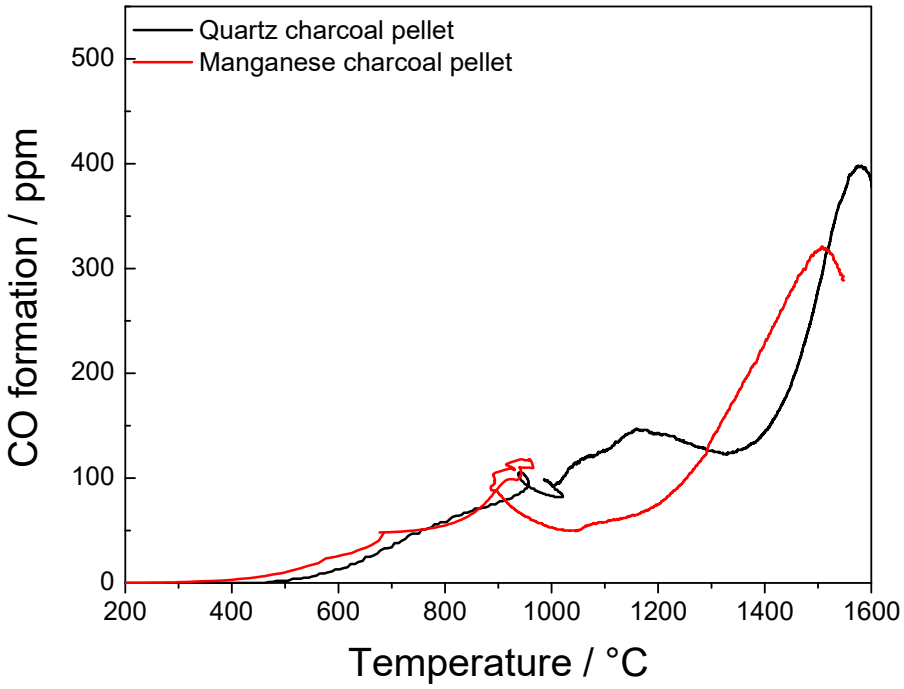

Figure 3: CO evolution of manganese and quartz charcoal pellets during pyrolysis.

The melting point of manganese oxides increased with the decreased oxidation state of manganese in the temperature range from 535°C (MnO_2) to 1945°C (MnO), whereas elemental manganese has a melting point of 1246°C [61]. Thus, the higher oxidation states of manganese can melt and react faster with the carbonaceous matrix of charcoal than the lower manganese oxidation states during the reduction. CO formation during the reduction of quartz charcoal pellets began at 1330°C with the maximum yield observed at 1580°C. In the present study, the temperature for the maximum CO yield was 100°C lower than temperatures reported in previous studies [62]. The decrease in the temperature required for maximum CO formation during

charcoal pellet conversion into the elemental metals emphasizes a key role of the feedstock on the reduction of ferroalloys.

3.4. Charcoal pellet reactivity

Figure 4 shows the differential weight loss curves for the 100 % volume fraction CO_2 gasification of spruce and oak charcoal pellets with a diameter of 3 mm. The DTG curves show a double peak in CO_2 gasification, indicating a heterogeneous char mixture with respect to the composition that leads to the differences in reactivity of the two constituents with less reactive carbon structure. The highest reaction rates of spruce charcoal pellets varied from 950 to 1010°C while that of the oak charcoal pellets occurred between 930 and 1010°C, indicating that feedstock origin had a minor effect on the char reactivity. The maximum reaction rates of spruce and oak charcoal pellets were observed nearly identically at 1300°C. In general, previous studies showed that the maximum reaction rates of charcoal pellets were similar to those of secondary heat treated biooil-charcoal blends [41]. The results show that differences in heat treatment temperature have more influence on charcoal reactivity than the feedstock composition.

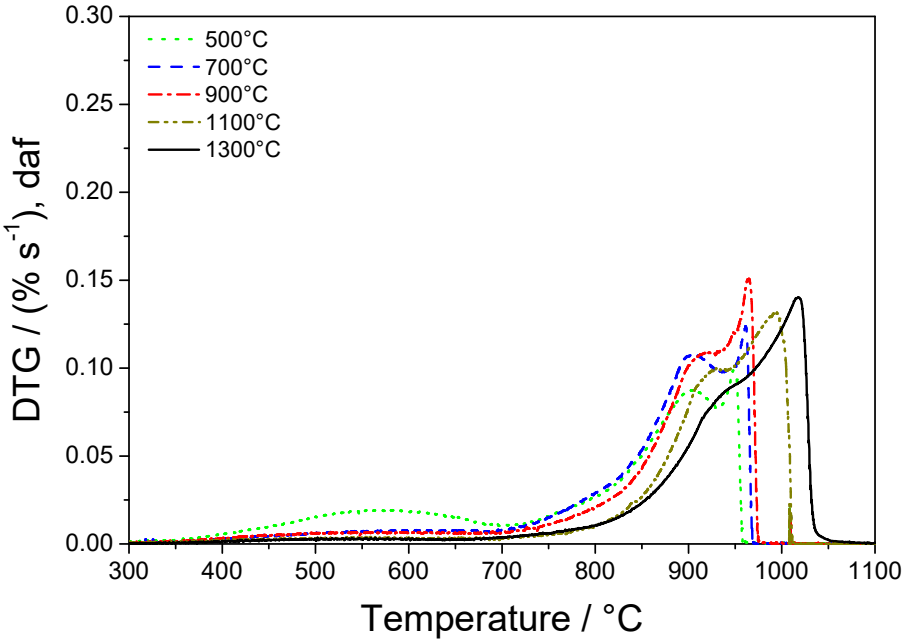

4(a): Spruce pellets

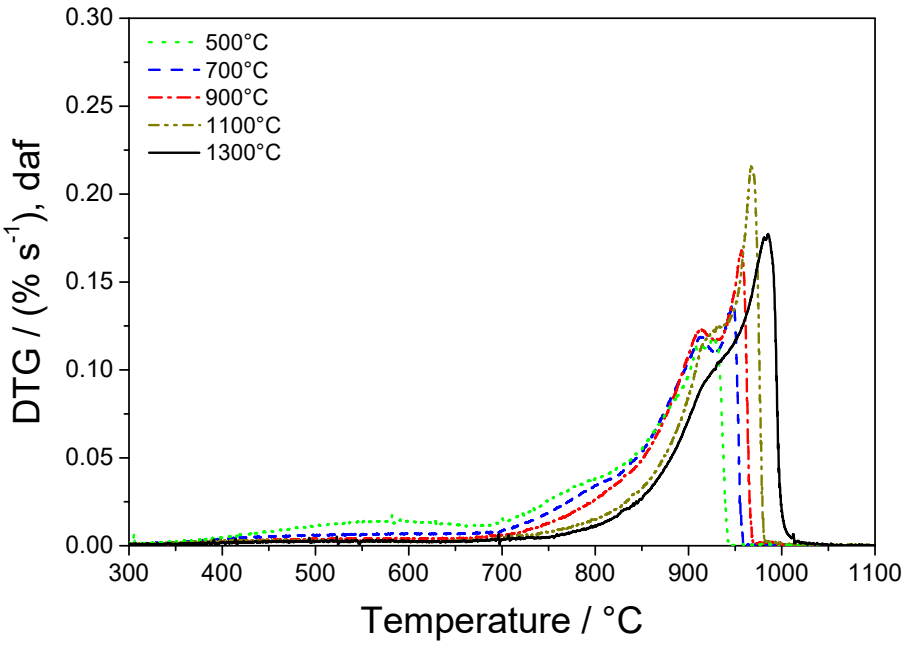

4(b): Oak pellets

Figure 4: DTG curves of charcoal pellets generated from (a) spruce and (b) oak and reacted in 100 % volume fraction CO_2.

3.5. Electrical resistivity

The electrical resistivity of the original charcoal and charcoal composite pellets with the included manganese oxide or quartz particles was investigated and summarized in Table 3. The charcoal was prepared at 700 or 900°C, then compressed in a pellet that was further dried and secondary heat treated (SHT) at 1300°C in the high temperature furnace. The electrical resistivity of manganese oxide charcoal pellets decreased from 1.7 to 0.35 Ωm, whereas the electrical resistivity of quartz charcoal pellets remained unchanged (≈ 0.4 Ωm).

Table 3: Electrical resistivity of manganese oxide or quartz charcoal pellets including standard deviation (σ).

	After compression		After drying		After SHT	
Material	Ωm	σ	Ωm	σ	Ωm	σ
non-treated charcoal pellet (700°C)	0.8	0.4	1.1	0.3	1.5	0.4
non-treated charcoal pellet (900°C)	0.01	0.03	0.02	0.03	0.02	0.05
MnO charcoal pellet	1.7	0.4	1.1	0.3	0.3	0.1
Quartz charcoal pellet	0.4	0.4	1.1	0.4	0.4	0.1

In comparison, the electrical resistivity of the original charcoal pellets increased from 0.8 to 1.5≈ 0.4 Ωm after heat treatment [41]. The electrical resistivity of these original charcoal particles decreased from 1.5 to 0.01 Ωm between 700 to 900°C and remained relatively constant during heat treatment up to 1300°C, emphasizing the importance of the role of temperature above 700°C.

3.6. Pellet shrinkage

Figure 5 shows silhouette areas of the original charcoal pellets from spruce and oak as well as the manganese oxide charcoal pellets using the heating microscope at temperatures up to 1200°C. The charcoal pellets shrunk when the primary pyrolysis temperature was exceeded. The distillation of biooil resulted in a loss of oil and the formation of solid coke. Interestingly, no swelling was observed on the surface of the charcoal pellets in the boiling range. The results indicate that incomplete pyrolysis was progressing even when the heat treatment temperature exceeded the final temperature of primary pyrolysis. Moreover, the evaporation of the lighter molecules from the biooil had no influence on the particle size or shape of the charcoal pellets. Spruce charcoal pellets decreased in size during CO_2 gasification at 900°C because the overall charcoal pellet reduction was limited by the Boudouard reaction 2 [63]:

$$CO_2(g) + C(s) = 2CO(g) \tag{2}$$

In contrast, the size of manganese oak charcoal pellets remained unchanged due to the high partial pressure of CO_2 according to reaction 3 [64]:

$$MnO(s) + CO(g) = Mn(s) + CO_2(g) \tag{3}$$

In general, a dilatation of manganese oxide charcoal pellets was observed when the sample reached the final temperature of 1200°C. The pellets formed whiskers at the outer surface when the temperature was increased to 1300°C and a residence time of 30 min, as shown in the supplemental material (Figure S-2). Structural changes were not observed at temperatures greater than 1300°C during experiments in the high temperature furnace confirming pre-

vious results [65] which suggested that the manganese ore could be reduced to the elemental manganese and further reacted to manganese (II) nitride at temperatures below 1300°C.

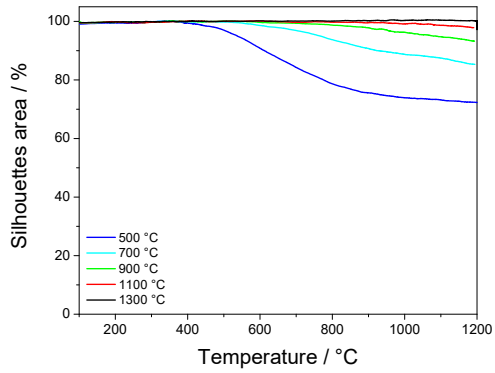

5(a): Original spruce pellets

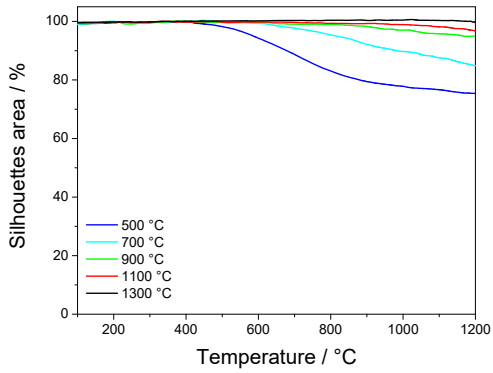

5(b): Original oak pellets

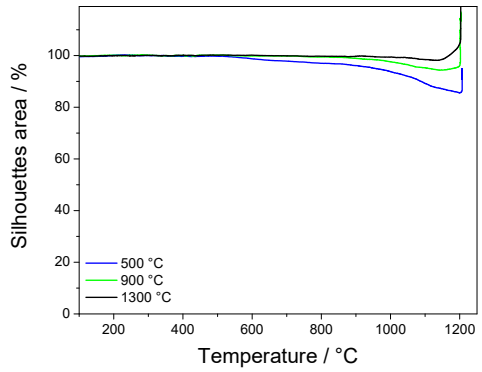

5(c): Spruce MnO charcoal pellet

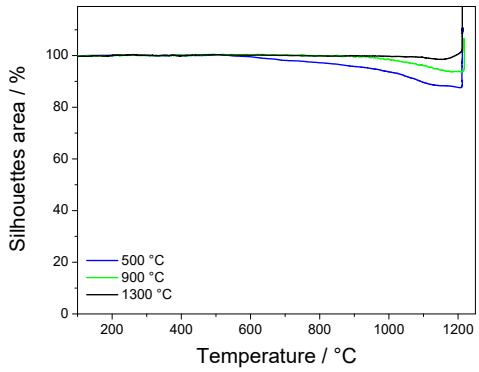

5(d): Oak MnO charcoal pellet

Figure 5: Percentage of silhouette area changes of original wood pellet and manganese oxide charcoal pellets in nitrogen atmosphere using the heating microscopy at temperatures up to 1200°C.

3.7. Thermodynamic calculations with FactSage

Equilibrium calculations of charcoal composite pellets were performed to investigate the formation of slag phases.

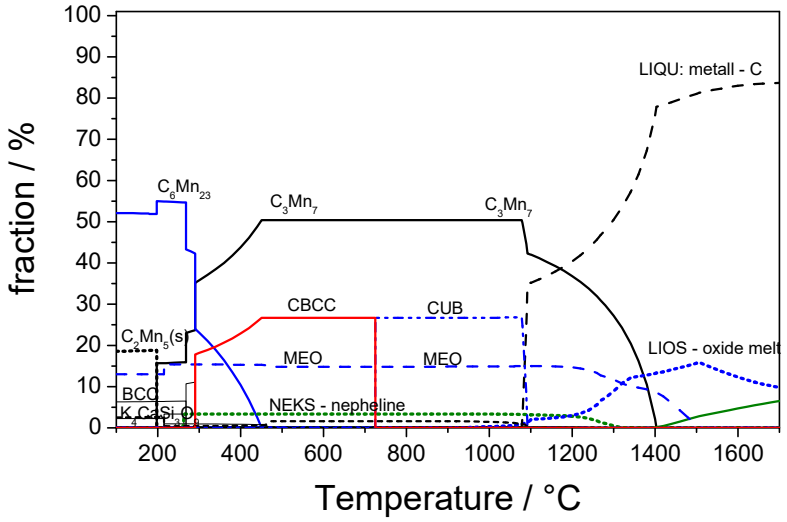

6(a): Manganese ore composite pellet

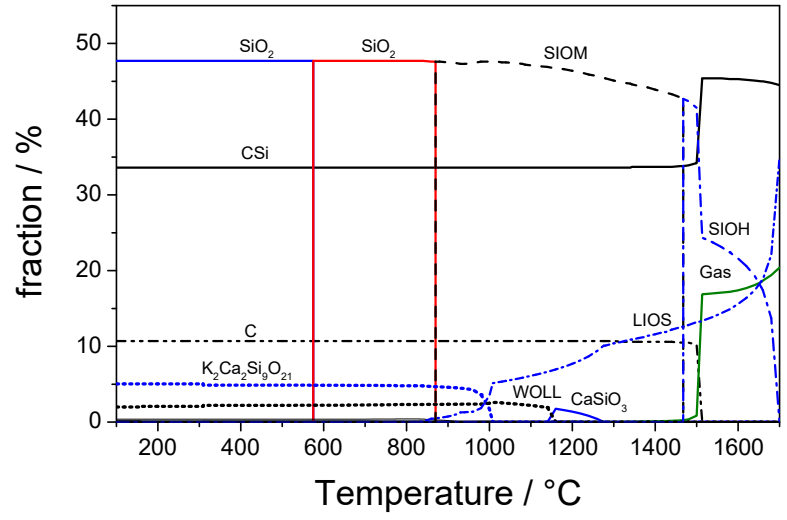

6(b): Silica composite pellet

Figure 6: Output results of FactSage calculation using the GTOX database with the main inorganic components of charcoal composite pellets containing MnO or quartz particles after heat treatment at 1650°C. The following abbreviations were used MEO (solid solution containing mostly MnO only), LIOS (oxide melt), CBCC and CUB (manganese-based solid solution phases), BCC (iron-based solid solution phase), SIOM (solid solution based on $SiO_{2,tridymite}$), SIOH (solid solution based on $SiO_{2,cristobalite}$) and WOLL (wollastonite).

The thermodynamic calculations showed that silicon carbides, silicon oxides, carbon and gas were the dominant phases formed during quartz charcoal pellet reduction, as shown in Figure 6. Manganese carbides were found along with silicates in manganese oxide charcoal pellets. The thermodynamic calculations showed a liquid elemental metal phase composed almost entirely of manganese with small amounts of carbon and other metals (Al, Fe), manganese carbide (C_3Mn_7) as well as solid solution based on manganese (II) oxides (MnO) were the dominant phases formed during the pyrolysis of MnO containing charcoal pellets in the temperature range from 1200 to 1300°C. Previous studies have shown the formation of manganese carbides in the temperature range from 800 to 1300°C, whereas manganese oxides and liquid oxides were formed at temperatures greater than 1200°C [66, 67]. The C_6Mn_{23} compound was formed for MnO/C ratios greater than 1/1.3, whereas C_3Mn_7 and carbon were formed during reduction with larger carbon excess ratios, confirming the previous results of Kononov et al. [68]. The equilibrium calculations demonstrate that C_3Mn_7 can be formed at temperatures up to 1400°C, whereas the dissociation of manganese carbides into liquid manganese alloys and graphite can occur at temperatures above 1300°C through peritectic reactions. The discrepancy between experiments and calculations can be explained by a lack of reliable thermodynamic information concerning phase relations between oxides and carbides in the available databases and also by the fact, that the calculations considered the equilibrium state only. MnO/C ratios lower than 1/1.3 provide sufficient amounts of carbon to completely reduce the manganese alloys based on the XRD results from previous studies of Shin et al. [69]. In the present study, the formation of

manganese carbides during reduction can be related to the slow cooling rate, according to Grimsley et al. [70].

3.8. X-ray diffraction

The charcoal was prepared at 900°C, compressed into a pellet with the MnO and SiO_2 particles using tar as a binder. Prior to the XRD analysis, the charcoal composite pellet was dried and secondary heat treated (SHT) at 1300°C.

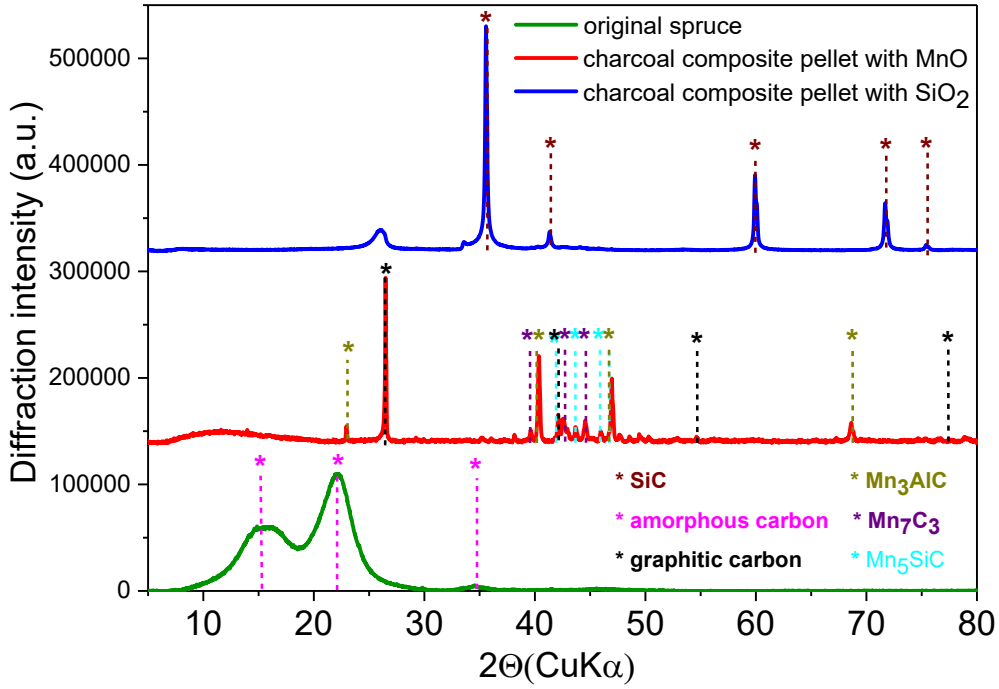

Figure 7: XRD measurements of original spruce, spruce charcoal pellet with MnO particles or with quartz particles after heat treatment.

The XRD analysis of the original spruce indicated the formation of a crystalline pattern corresponding to the cellulose structure, as shown in Fig-

ure 7. The broad reflections at 15, 22.5 and 35° show the development of a crystalline cellulose phase [71, 72]. The XRD results showed that charcoal pellets with MnO particles exhibit reflections from graphitic carbon indicating the progress towards graphitization with increasing heat treatment temperature. In addition, charcoal pellets with MnO particles show reflections from orthorhombic manganese carbides (Mn_5SiC and Mn_7C_3) and cubic manganese carbide (Mn_3AlC), whereas the charcoal quartz pellets show sharp and narrow reflections from silicon carbide [73, 74]. The formation of silicon carbides during high-temperature pyrolysis of charcoal quartz pellets is due to the decomposition of charcoal carbon onto the quartz particles [62].

3.9. Microscopy

The external surface structure of manganese oxide charcoal pellet after reduction was studied using microscopy, as shown in Figure 8. Structural changes to composite charcoal pellets arising from reduction were investigated at locations on the top, bottom and side of the pellet. Figure 8(a) shows that the porosity of the manganese alloy particles increased after heat treatment. In addition, Figure 8(b) shows the formation of a metal skeleton with the large voids that probably contain manganese carbides due to the large amount of carbon detected during SEM-EDS analysis. The original structure of the charcoal particles was only observed at locations where manganese oxide particles were not incorporated, as shown in Figures 8(c)-8(d). Figure 9 shows a cross section of a manganese oxide charcoal pellet. The high temperature reduction of manganese oxides led to the formation of large voids inside the particle, which were filled with the reacting charcoal material.

8(a): Bottom

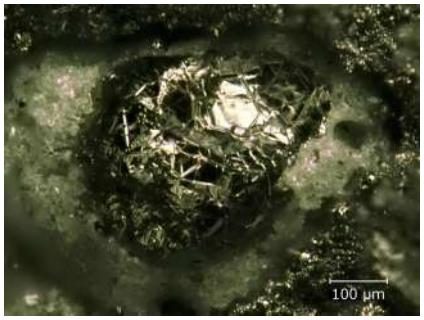

8(b): Bottom zoom

8(c): Top

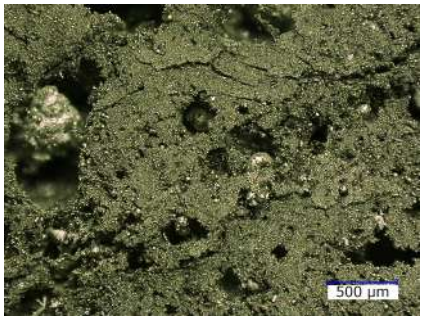

8(d): Side

Figure 8: Optical microscopy of manganese composite pellets at the bottom, at the top and on the side of the pellet.

Moreover, Figure 9 indicates the formation of different liquefied metal phases. The dissolution of carbon into the metal slag has been observed at the boundary layer between the slag and charcoal particles [75]. Figure 9 shows that the structure of the quartz charcoal pellets remained unchanged after their reduction at 1650°C. The charcoal structure can be visually distinguished from the unreacted quartz particles. However, an additional solid carbon structure was formed inside the charcoal structure related to the formation of silicon oxides during the reduction. Previous studies have shown that amorphous SiO_2 could be formed as a decomposition product of gaseous

SiO at lower temperatures. The gaseous SiO can be produced in advance in an oxygen-deficient atmosphere at higher temperatures according to reaction 4 [76].

$$SiO_2(s) + Si(l) = 2SiO(g) \tag{4}$$

The additional layer of silicon carbides could block the pellet surface for further consecutive reactions, resulting in reduced formation of CO at 1650°C [77]. Figure 9 shows copper particles which originate from the sample metallurgical preparation.

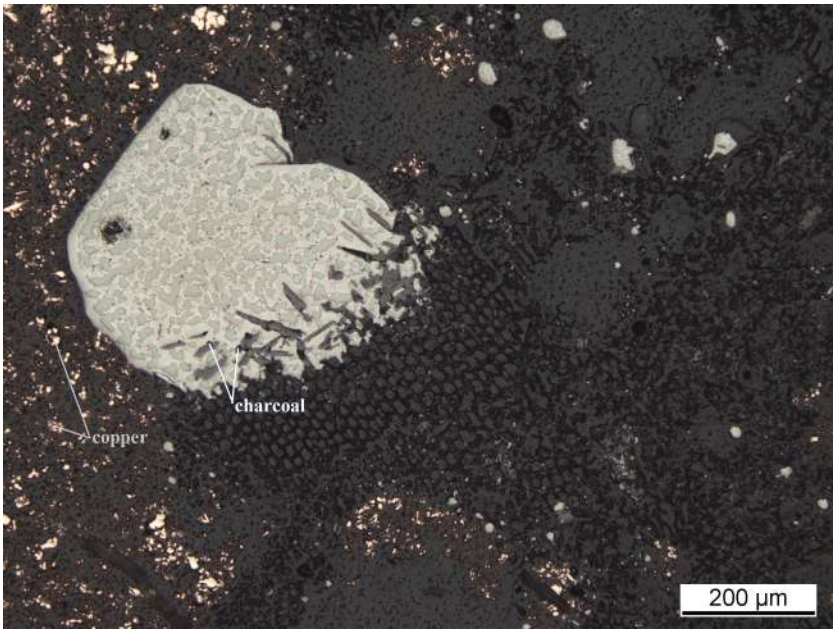

Figure 9: Cross section of the manganese charcoal pellet.

The elemental composition of the charcoal composite pellets is summarized in the supplemental material (Table S-3). The mapping areas of the SEM-EDS analysis are schematically shown in the supplemental material

(Figure S-5 and Figure S-6). The results of elemental analysis using SEM-EDS showed that iron, aluminum and silicon were detected in the reduced manganese oxide charcoal pellet. The metal skeleton was embedded into the carbonaceous charcoal matrix, whereas oxygen was mainly observed in the charcoal enriched spots. Moreover, the high quantities of carbon and manganese suggest that manganese oxides were reduced to manganese and manganese carbides during high temperature treatment.

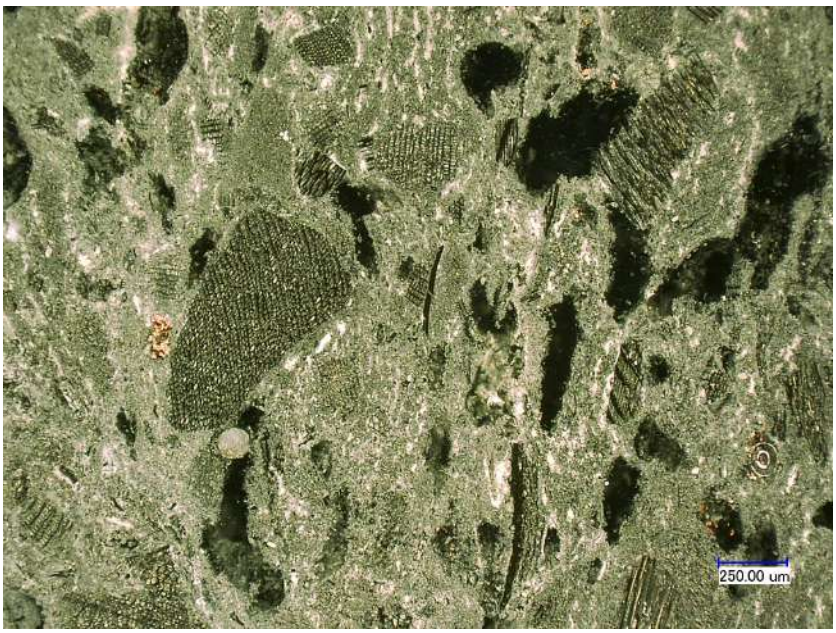

Figure 10: Optical microscopy of quartz charcoal pellets.

The iron inclusions in the manganese charcoal pellets suggest the formation of iron carbides which belong to the eutectic carbides with a melting point at 1153°C [60]. The liquefied carbon and iron from the reduction can crystallize to eutectic graphite during cooling [78]. The elemental analysis of the reduced quartz charcoal pellets indicated that the composition changed

only slightly during the reduction due to the high oxygen content in the charcoal particles. However, the high mass loss of the quartz charcoal pellets (47 %) was an indication of the decomposition of charcoal and biooil and the reduction of quartz based on the results above (section 3.2).

3.10. X-ray microtomography

Figure 11 shows the 2D and 3D cross-sectional slices obtained from XμCT measurements for non-treated and heat treated charcoal pellets. The characteristic features of charcoal particles are observed for all scanned samples. The spatial resolution of 3.5 μm is sufficient for observing most features of the charcoal particles and binder, providing physically reasonable structural assessments. The XμCT images indicated that the charcoal particles in heat treated pellets were more porous than charcoal particles in untreated pellets. The greater level of voids, obtained with the treated pellets than in non-treated pellets reflects the higher porosity of treated charcoal pellets, confirming the previous results of Trubetskaya et al. [22]. The porosity increase from 0.5 to 1.4 % with the temperature treatment in the charcoal pellets was mostly related to the release of volatiles during the heat treatment. The XμCT images indicated that solid manganese oxide particles melt and formed large voids during the reduction of charcoal composite pellets, as shown in Figure 12. The low level of voids in the carbonaceous matrix of charcoal pellets after reduction reflects the reaction of manganese oxide and organic charcoal matter into elemental manganese, manganese carbides, etc. In addition, the increased porosity from 50.1 to 84.7 % in the manganese charcoal pellets was mostly due to the transformation of manganese oxides to elemental manganese and the gaseous products released during the

reduction.

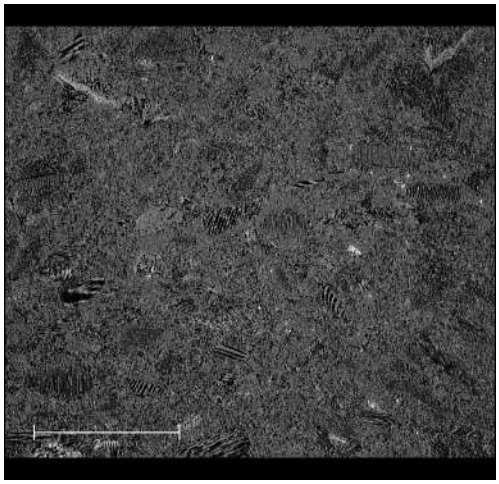

11(a): 2D projection of non-treated pellet

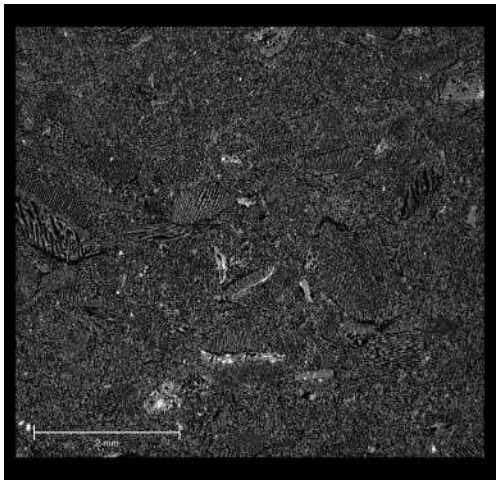

11(b): 2D projection of heat treated pellet

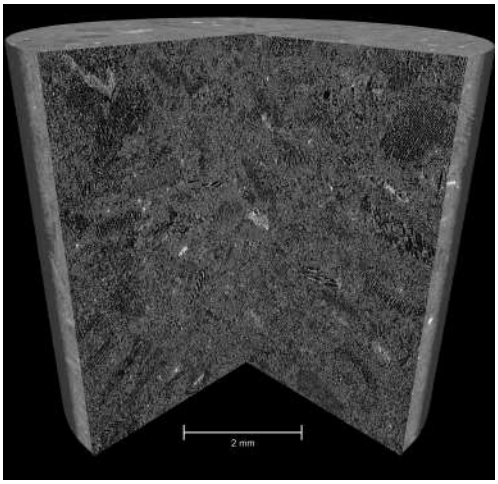

11(c): 3D projection of non-treated pellet

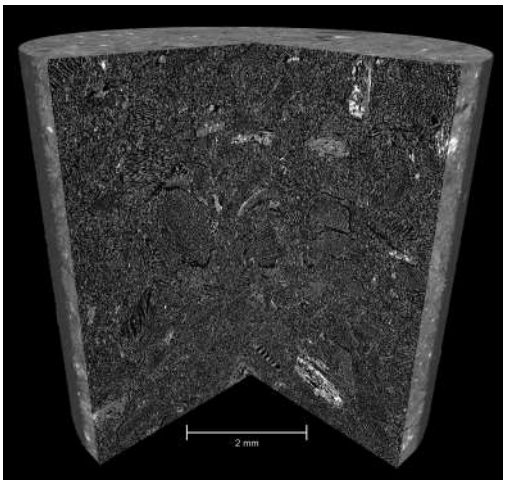

11(d): 3D projection of heat treated pellet

Figure 11: XμCT imaging analysis of non-treated and heat treated charcoal pellets.

The XμCT images indicate that the quartz particles in charcoal composite pellets remained unchanged in terms of their shape and size, corresponding to the optical microscopy results. In addition, the quartz particles

remained solid and the border between quartz particles and charcoal matrix is visible indicating less transformations in quartz particles during reduction compared to the heat treatment of manganese charcoal pellets. The porosity of quartz charcoal pellets increased only slightly from 43.1 to 53.7 %.

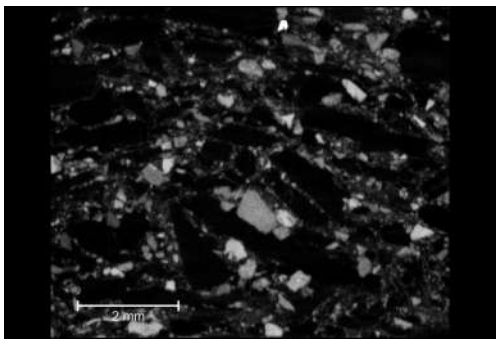

12(a): 2D projection of raw Mn charcoal pellet

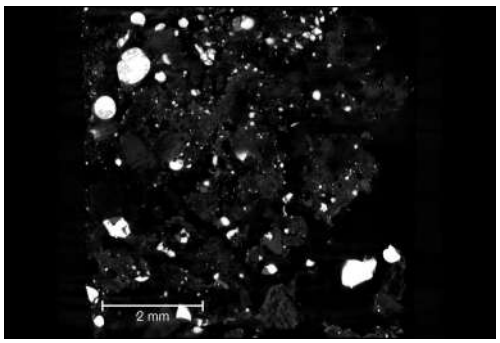

12(b): 2D projection of heat treated Mn charcoal pellet

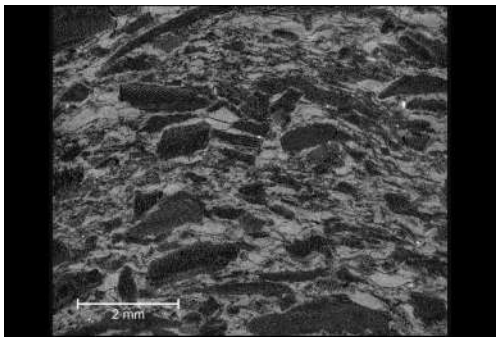

12(c): 2D projection of raw quartz charcoal pellet

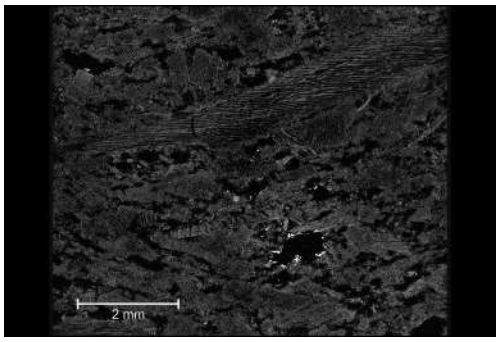

12(d): 2D projection of heat treated quartz charcoal pellet

Figure 12: XμCT imaging analysis of raw and heat treated manganese or quartz charcoal pellets.

4. Conclusion

The novelty of this work is the experimental demonstration that the solid yield, electrical resistivity and conversion of ferroalloys to the elemental metals can be improved by the addition of biooil as a binder to the charcoal composite pellets. Softwood and hardwood were converted into renewable carbonaceous reductants using pyrolysis treatment. The experiments in the heating microscope and high-temperature furnace showed that the solid yields were 5-55 % greater during reduction of the original charcoal pellets than during the pyrolysis of the charcoal composite pellets. The charcoal pellets developed a similar reactivity to the charcoal-biooil blends with with the highest reactivity observed between 930 to 1010°C and thus, remained more reactive than fossil-based coke where the maximal reaction rate was at 1220°C. The electrical resistance of pellets from charcoal prepared at 700°C was 100 times greater than that of composite pellets prepared at 900°C. Moreover, the electrical resistance of both manganese oxide and quartz charcoal pellets decreased to 0.4 Ωm emphasizing the importance of secondary heat treatment and type of included ore on the electrical properties of bioreductants. The porosity of charcoal pellets was increased by approximately 30 % during transformation of manganese oxides to elemental manganese, whereas the porosity increased only by 10 % during reduction of quartz charcoal pellets. The changes in the macroporosity of the charcoal composite pellets during reduction emphasize both the importance of ash transformation reactions related to present of alkali metals in original feedstock and included ore particles. The X-ray diffraction, X-ray microtomography, SEM-EDS and thermodynamic calculations showed that the carbides and oxides were dom-

inating phases formed during the reduction of charcoal composite pellets indicating the high degree of conversion of metal oxides to elemental metals. The find- ings of this study emphasize the potential use of biocarbon-based composite pellets in the ferroalloy industry with concomitant improvement in charcoal transportation and storage.

Acknowledgements

The authors gratefully acknowledge financial support from Elkem AS, Saint Gobain Ceramic Materials AS, and Eramet Norway AS. The authors would like to thank Ivan Josipovic, from the Radiation Physics group of the University of Ghent, for performing the μCT scans.

References

[1] A. Steinfeld, High-temperature solar thermochemistry for CO_2 mitigation in the extractive metallurgical industry, Energy 22 (2) (1997) 311–6.

[2] E. Balomenos, D. Panias, I. Paspaliaris, Energy and Exergy Analysis of the Primary Aluminum Production Processes: A Review on Current and Future Sustainability, Min Proc Extr Met Rev 32 (2) (2011) 69–89.

[3] S. Dutta, Iron ore–coal composite pellets/briquettes as new feed material for iron and steelmaking, Mat Sci Eng Int J 1 (2017) 10–3.

[4] Riva L, Surup GR, Buø TV, Kofoed Nielsen H, A study on densified biochar as carbon source in the silicon and ferrosilicon production, Energy 65 (2019) 355–60.

[5] Riva L, Kofoed Nielsen H, Skreiberg Ø, Wang L, Bartocci P, Barbanera M and etc., Analysis of optimal temperature, pressure and binder quantity for the production of biocarbon pellet to be used as a substitute for coke, Appl Energy 256 (2019) 1–16.

[6] S. Olsen, M. Tangstad, T. Lindstad, Production of Manganese Ferroalloys, Tapir Akademisk Forlag, 2007.

[7] R. Nascimento, M. Mourao, J. Capocchi, Reduction-swelling behaviour of pellets bearing iron ore and charcoal, Can Metall Quart 37 (5) (1998) 441–8.

[8] M. Tangstad, D. Leroy, E. Ringdalen, Behaviour of agglomerates in

ferromanganese production, INFACON XII, Hensinki, Finland (2010) 457–66.

[9] H. Yoshikoshi, O. Takeuchi, T. Miyashita, T. Kuwana, K. Kishikawa, Development of Composite Cold Pellet for Silico-Manganese Production, Trans ISIJ 24 (6) (1984) 492–7.

[10] C. Harman, N. Rama Rao, Use of sintered pellets in production of high carbon ferrochrome, INFACON XI, New Delhi, India (2007) 67–74.

[11] B. Zhang, Z. Xue, Kinetics Analyzing of Direction Reduction on Manganese Ore Pellets Containing Carbon, IJNM 2 (2013) 116–20.

[12] S. Jayakumari, M. Tangstad, Carbon materials for silicomanganese reduction, INFACON XIV, Kiev, Ukraine (2015) 374–81.

[13] T. Lintumaa, H. Krogerus, P. Jokinen, Factors affecting the reducibility of sintered chromite pellets and chromite lump ore, INFACON XI, New Delhi, India (2007) 75–84.

[14] T. Brynjulfsen, M. Tangstad, Melting and reduction of manganese sinter and pellets, INFACON XIII, Almaty, Kazakhstan (2013) 137–47.

[15] S. Mishra, G. Roy, Effect of Amount of Carbon on the Reduction Efficiency of Iron Ore-Coal Composite Pellets in Multi-layer Bed Rotary Hearth Furnace (RHF), Metall Mat Trans B 47 (4) (2016) 2347–56.

[16] E. Kasai, T. Kitajima, T. Kawaguchi, Carbothermic Reduction in the Combustion Bed Packed with Composite Pellets of Iron Oxide and Coal, ISIJ Int 40 (9) (2000) 842–9.

[17] A. Mašlejová, Utilization of biomass in ironmaking, Metal (2013) 122–7.

[18] K. Papadikis, S. Gu, A. Bridgwater, CFD modelling of the fast pyrolysis of biomass in fluidised bed reactors: Modelling the impact of biomass shrinkage, Chem Eng J 149 (1-3) (2009) 417–27.

[19] Somerville MA, The Strength and Density of Green and Reduced Briquettes Made with Iron Ore and Charcoal, J Sust Met 2 (3) (2016) 228–38.

[20] Surup GR, Hunt AJ, Budarin VL, Attard T, Forsberg F, Trubetskaya A and etc., The effect of wood composition and supercritical CO_2 extraction on charcoal production in ferroalloy industries, Energy .

[21] Trubetskaya A, Deike R, Foppe M, Heidelmann M, Surup GR, Schubert D and etc., The effect of feedstock origin and temperature on the structure and reactivity of char from pyrolysis at 1300–2800°C, Fuel 235 (2018) 306–16.

[22] Trubetskaya A, Leahy JJ, Yazhenskikh E, Müller M, Layden P, Johnson R and etc., Characterization of woodstove briquettes from torrefied biomass and coal, Energy 171 (2019) 853–865.

[23] R. Sah, S. Dutta, Effects of Binder on the Properties of Iron Ore-Coal Composite Pellets, Min Process Extr Met Rev 31 (2) (2010) 73–85.

[24] J. Pal, A. Ayyandurai, A. Ammasi, S. Hota, V. Koranne, T. Venugopalan, Improving reducibility of iron ore pellets by optimization of physical parameters, J Min Metall Sect B Metall 53 (2016) 1–10.

[25] C. Seaton, J. Foster, J. Velasco, Structural Changes Occurring during Reduction of Hematite and Magnetite Pellets Containing Coal Char, Trans ISIJ 23 (6) (1983) 497–503.

[26] N. Yunos, N. Aziz, A. Ismail, M. Idris, Reduction Behaviour of Iron Ores by Agricultural Waste Chars, Mat Sci Forum 819 (2015) 31–6.

[27] C. Seaton, J. Foster, J. Velasco, Reduction Kinetics of Hematite and Magnetite Pellets Containing Coal Char, Trans ISIJ 23 (6) (1983) 490–6.

[28] M. Bahgat, K. Abdel Halim, H. El-Kelesh, M. Nasr, Metallic iron whisker formation and growth during iron oxide reduction: K_2O effect, Ironmak Steelmak 36 (5) (2009) 379–87.

[29] Gasik M, Handbook of Ferroalloys: Theory and Technology, Butterworth-Heinemann, 2013.

[30] Donskoi E, Olivares RI, McElwain DLS, Wibberley LJ, Experimental study of coal based direct reduction in iron ore/coal composite pellets in a one layer bed under nonisothermal, asymmetric heating, Ironmaking Steelmaking 33 (1) (2006) 24–9.

[31] Wang Q, Yang Z, Tian J, Li W, Sun J, Mechanisms of reduction in iron ore coal composite pellet, Ironmak Steelmak 24 (6) (1997) 457–60.

[32] Wang Q, Yang Z, Tian J, Li W, Sun J, Reduction kinetics of iron ore-coal pellet during fast heating, Ironmak Steelmak 25 (6) (1998) 443–7.

[33] Praes GE, Dimas de Arruda J, Rocha Lemos L, Parreiras Tavares R, Assessment of iron ore pellets production using two charcoals with different content of materials volatile replacing partially anthracite fines, J Mat Res Tech 8 (1) (2019) 1150–60.

[34] Filho AT, Lange LC, Caldeira Bandeira de Melo G, Praes GE, Pyrolysis of chromium rich tanning industrial wastes and utilization of carbonized wastes in metallurgical process, Waste Manage 48 (2016) 448–56.

[35] Longbottom RJ, Monaghan BJ, Nightingale SA, Mathieson JG, Strength and bonding in reduced ironsand-coal compacts, Ironmak Steelmak 40 (5) (2013) 381–9.

[36] Longbottom RJ, Monaghan BJ, Mathieson JG, Development of a bonding phase within titanomagnetite-coal compacts, ISIJ Int 53 (7) (2013) 1152–60.

[37] Pandey BK, Sharma T, Reducing agents and double-layered iron ore pellets, Int J Miner Process 59 (2000) 295–304.

[38] Sharma T, Reduction of double layered iron ore pellets, Int J Miner Process 49 (1997) 201–6.

[39] Fruehan RJ, The rate of reduction of iron oxides by carbon, Mat Trans B 8 (1) (1977) 279–86.

[40] Tien RH, Turkdogan ET, Mathematical analysis of reactions in metal oxide/carbon mixtures, Met Trans B 8 (1) (1977) 305–13.

[41] G. Surup, T. Vehus, P. Eidem, A. Trubetskaya, H. Nielsen, Characterization of renewable reductants and charcoal-based pellets for the use in ferroalloy industries, Energy 167 (2019) 337–45.

[42] G. Surup, H. Nielsen, M. Heidelmann, A. Trubetskaya, Characterization and reactivity of charcoal from high temperature pyrolysis (800-1600°C), Fuel 235 (2019) 1544–54.

[43] H. Suopajärvi, A. Kemppainen, J. Haapakangas, T. Fabritius, Extensive review of the opportunities to use biomass-based fuels in iron and steelmaking processes, J Clean Prod 148 (2017) 709–34.

[44] L. Sun, J. Wang, E. Bonaccurso, Conductivity of individual particles measured by a microscopic four-point-probe method, Sci Rep 3 (2013) 1–5.

[45] L. van der Pauw, A Method of Measuring Specific Resistivity and Hall Effect of Discs of Arbitrary Shape, Philips Res Rep 13 (1) (1958) 1–9.

[46] C. Bale, E. Belisle, P. Chartrand, S. Decterov, G. Eriksson, A. Gheribi, etc., FactSage thermochemical software and databases, 2010-2016, Calphad 54 (2016) 35–53.

[47] E. Yazhenskikh, T. Jantzen, K. Hack, M. Müller, A new multipurpose thermodynamic database for oxide systems, Raplavy/Melts 2 (2) (2019) 116–24.

[48] K. Hack, T. Jantzen, M. Müller, E. Yazhenskikh, G. Wu, A novel thermodynamic database for slag systems and refractory materials, Proceedings 5th Int Congress Sci Tech Steelmaking, ICS Dresden (2012) 1–15.

[49] M. Dierick, D. Van Loo, B. Masschaele, M. Boone, L. Van Hoorebeke, A LabVIEW based generic CT scanner control software platform, J X-ray Sci Technol 18 (4) (2010) 451–61.

[50] B. Masschaele, M. Dierick, D. Van Loo, M. Boone, L. Brabant, E. Pauwels, etc., HECTOR: A 240kV micro-CT setup optimized for research, J Phys Conf Ser 463 (1) (2013) 1–4.

[51] J. Vlassenbroeck, M. Dierick, B. Masschaele, V. Cnudde, L. Van Hoorebeke, P. Jacobs, Software tools for quantification of X-ray microtomography at the UGCT, Proceedings 5th Int Congress Sci TechSteelmaking, ICS Dresden (2012) 1–15.

[52] A. Sluiter, B. Hames, R. Ruiz, C. Scarlata, J. Sluiter, D. e. a. Templeton, Determination of Structural Carbohydrates and Lignin in Biomass. Golden (CO): National Renewable Energy Laboratory; 2011 July Report No. NREL/TP-510-42618. Contract No.: DE-AC36-08-GO28308 .

[53] S. Willför, J. Hemming, A. Leppänen, Analysis of extractives in different pulps - Method development, evaluation, and recommendations. Finland: Åbo Akademi University, Laboratory of Wood and Paper Chemistry; 2004-2009 Report No. B1 of the EU COST E41 action "Analytical tools with applications for wood and pulping chemistry" .

[54] B. Hames, R. Ruiz, C. Scarlata, J. Sluiter, A. Sluiter, Preparation of Samples for Compositional Analysis. Golden (CO): National Renewable

Energy Laboratory; 2011 June Report No. NREL/TP-510-42620. Contract No.: DE-AC36-99-GO10337 .

[55] K. Thammasouk, D. Tandjo, M. Penner, Influence of Extractives on the Analysis of Herbaceous Biomass, J Agric Food Chem 45 (1997) 437–43.

[56] M. Kumar, R. Gupta, Influence of carbonization conditions on physical properties of Acacia and Eucalyptus wood chars, Trans Ind Inst Met 46 (6) (1993) 345–52.

[57] C. Brewer, V. Chuang, C. Masiello, H. Gonnermann, X. Gao, B. Dugan, etc., New approaches to measuring biochar density and porosity, Biomass Bioenergy 66 (2014) 176–85.

[58] A. Veksha, H. McLaughlin, D. Layzell, J. Hill, Pyrolysis of wood to biochar: Increasing yield while maintaining microporosity, Biores Tech 153 (2014) 173–9.

[59] K. Abdel Halim, M. Bahgat, M. Morsi, K. El-Barawy, Pre-reduction of manganese ores for ferromanganese industry, Ironmak Steelmak 38 (4) (2011) 279–84.

[60] F. Sesen, Practical reduction of manganese oxide, Int J Chem Eng Appl 1 (1) (2017) 1–2.

[61] L. Staffansson, On the Mn-MnS phase diagram, Met Mat Trans B 7 (1) (1976) 131–4.

[62] F. Li, M. Tangstad, I. Solheim, Quartz and carbon black pellets for silicon production, INFACON XIV, Kiev, Ukraine (2015) 390–401.

[63] W. Rankin, J. Wynnyckyj, Kinetics of reduction of MnO in powder mixtures with carbon, Met Mat Trans B 28 (2) (1997) 307–19.

[64] W. Rankin, J. Van Deventer, The kinetics of the reduction of manganous oxide by graphite, J South African Inst Min Met 80 (7) (1980) 239–47.

[65] M. Lyutaya, A. Goncharuk, Manganese nitrides, Sov Powder Metall 16 (3) (1977) 208–12.

[66] M. Yastreboff, O. Ostrovski, S. Ganguly, Carbothermic Reduction of Manganese from Manganese Ore and Ferromanganese Slag, INFACON VIII, Beijing, China (1998) 263–70.

[67] C. Akil, A. Geveci, Optimization of Conditions to Produce Manganese and Iron Carbides from Denizli-Tavas Manganese Ore by Solid State Reduction, Turkish J Eng Env Sci 32 (2008) 125–31.

[68] R. Kononov, O. Ostrovski, S. Ganguly, Carbothermic solid state reduction of manganese ores, INFACON XI, New Delhi, India (2007) 258–67.

[69] H. Shin, B. Lee, H. Lee, Y. Lee, Mechanism of carbothermic reduction of Mn oxide powder, INFACON XIII, Almaty, Kazakhstan (2013) 621–9.

[70] W. Grimsley, J. See, R. King, Mechanism and rate of reduction of Mamatwan manganese ore fines by carbon, S African Inst Mining Metal 78 (3) (1977) 51–62.

[71] M. Wada, Y. Nishiyama, H. Chanzy, T. Forsyth, P. Langan, The structure of celluloses, Adv X-ray Analysis 51 (2008) 138–44.

[72] A. French, Idealized powder diffraction patterns for cellulose polymorphs, Cellulose 21 (2) (2014) 885–96.

[73] R. Schwarz, D. McCallum, Analysis of Ferrosilicon and Silicon Carbide by an X-ray Fluorescence Fusion Method - An X-ray Diffraction Investigation of the Preliminary Oxidation, Anal Comm 34 (1997) 165–9.

[74] S. Moustafa, M. Morsi, A. Alm El-Din, Formation of silicon carbide from rice hulls, Can Metall Quar 36 (5) (1997) 355–8.

[75] R. Braga, C. Takano, M. Mourao, Prereduction of self-reducing pellets of manganese ore, Ironmak Steemak 34 (4) (2007) 279–84.

[76] R. Deike, Reaktion zwischen flüssigem Silicium and Graphit sowie Siliciumnitrid im Hinblick auf neuartige Verfahren zur Raffination und Kristallisation von Silicium für Solarzellen. Doctoral thesis, Technical University of Clausthal, 1991.

[77] P. Pistorius, Reductant selection in ferro-alloy production: The case for the importance of dissolution in the metal, J South African Inst Min Met 102 (1) (2002) 33–6.

[78] F. Neumann, Theorien über das Impfen, Giesserei 83 (14) (1996) 11–15.